Open Access Online Journal on Astronomy and Astrophysics
Acta Astrophysica Taurica
www.astrophysicataurica.org

Acta Astrophys. Tau. 7(3), 5–14 (2026) EDN: JUNFSO

On the feasibility of solar sub-terahertz flare observations with the RATAN-600 radio telescope

V.B. Khaikin[1], G.A. Makoev[1], V.V. Smirnova[2]

[1] Special Astrophysical Observatory RAS (Saint-Petersburg department), Pulkovskoe sh. 65, Saint Petersburg, 196140, Russia
e-mail: vkhstu@mail.ru
[2] Crimean Astrophysical Observatory, Nauchny 298409
e-mail: vvsvid.smirnova@yandex.ru

Received 18 October 2023

ABSTRACT

We present a technique for observing solar sub-terahertz flares (STFs) with the RATAN-600 radio telescope. STF observations are proposed to be carried out during the routine multi-azimuth observations of the Sun with a reduced aperture at a frequency of 93 GHz.

The expected beam patterns of the antenna system at frequencies of 30, 93, and 140 GHz (10, 3, and 2 mm) were calculated taking into account possible errors of the element surfaces, errors in their mutual alignment, as well as the primary feed placed off-focus. Two-dimensional convolutions between the beam patterns and the solar disk model were obtained, one-dimensional scans of which correspond to the expected radio images of the Sun from RATAN-600. The expected STFs were assessed with respect to the model according to which sub-terahertz emission is generated due to the thermal bremsstrahlung mechanism of optically thick plasma in the chromosphere and the transition region of the Sun.

We propose simultaneous STF observations with RATAN-600 in a frequency range of 1–100 GHz and the Bauman Moscow State Technical University RT-7.5 radio telescope at frequencies of 93 and 140 GHz. Such cooperative multifrequency observations will make it possible to clarify the W-shaped spectrum of STFs in the decimeter, centimeter, and millimeter wavelength ranges and to elucidate the nature of sub-terahertz emission from solar flares with a positive spectral slope.

Key words: radio telescope, solar activity, sub-terahertz flares

1 Introduction

The radio flux density spectrum of solar flares in the centimeter (cm) wavelength range typically exhibits a positive slope at low frequencies and a negative slope at high frequencies (Kundu, Vlahos, 1982). One of the mechanisms generating centimeter emission from solar flares is the gyrosynchrotron mechanism. The shape of the gyrosynchrotron spectrum in the cm wavelength range allows one to identify the regions of optically thin and optically thick emission located on either side of the spectral maximum. The positive slope of the gyrosynchrotron spectrum in the low-frequency domain is determined by absorption that causes a decrease in spectral intensity with decreasing frequency, while the negative spectral slope in the high-frequency domain follows a power law and is determined by the energy distribution of accelerated electrons (Kupriyanova et al., 2020). Such a spectrum describes the behavior of accelerated particles in a magnetic field; these are generated during a flare and propagate downward from the solar corona, where they are decelerated in the dense layers of the solar atmosphere. This process is accompanied by chromospheric plasma evaporation that follows the impulsive phase of the flare and by enhancement of sub-terahertz (sub-THz) emission.

One of the major challenges for solar astrophysics in the 21st century has been the need to explain the intense emission from solar flares in the sub-THz wavelength range (0.1–1 THz) with a positive spectral slope (Stepanov, 2019), first detected at 250 GHz (Clark, Park, 1968). Numerous models describing a positive STF spectrum have been proposed to date, but none fully satisfies the observational results (Tsap et al., 2016).

The most significant instrumental contribution to the detection and study of STFs has been made by the Solar Submillimeter Telescope (SST), a 1.5-m diameter instrument located in the Argentine Andes at an altitude of 2550 m (Kaufmann et al., 2000), and the KOSMA submillimeter telescope, a 3-m diameter instrument located in the Swiss Alps at an altitude of 3135 m (Lüthi et al., 2004). In the Russian Federation, STFs are regularly observed with the Bauman Moscow State Technical University

RT-7.5 radio telescope at frequencies of 93 and 140 GHz with angular resolutions of 2.5 and 1.5 arcmin, respectively (Tsap et al., 2018).

At present, STFs are assumed to be of both thermal and nonthermal origin (Krucker et al., 2013). The sources of thermal sub-THz emission from flares with a positive spectral slope (α = 0.5–3.4) may be flaring ribbons with an area of ~1000 (arcsec)^2, well visible in the extreme ultraviolet (Kontar et al., 2018). In the mentioned paper, the authors presumed that sub-THz emission is generated via the thermal bremsstrahlung mechanism (free-free emission) of optically thick plasma located in the chromosphere and transition region, heated by nonthermal electrons or ions. As a result of flare heating of the chromosphere, plasma evaporates and fills coronal loops, where the emission becomes optically thick. Whereas plasma in the temperature range 0.1–1 MK produces enhanced sub-THz emission. However, such an interpretation implies the occurrence of a sub-terahertz Neupert effect, which is not observed in all flares (Smirnova et al., 2021). Moreover, the sources of sub-THz and extreme ultraviolet flare emission do not always coincide, as particularly demonstrated in Skokić et al. (2023). Furthermore, the thermal emission mechanism can explain neither pulsations in the sub-THz emission profiles with a period of 0.2 to 4 sec, with a flare duration of 2 to 10 min, nor the W-shaped spectrum (Stepanov, 2019).

On the other hand, STF sources of nonthermal origin are assumed to be compact (Kaufmann et al., 2009). The nonthermal mechanism of STF emission require anomalously high magnetic fields (exceeding 3000 G), heating of the solar chromosphere to coronal temperatures of 10^6–10^{10} K, and acceleration of electrons to energies of ~1 MeV. Modern nonthermal models of the flare process imply that the maximum of flares at frequencies above 100 GHz is produced by the gyrosynchrotron emission mechanism (Fleishman, Kontar, 2010). Electron acceleration may also occur in the chromosphere in inductive electric fields due to the Rayleigh–Taylor instability (Zaitsev, Stepanov, 2015), providing heating of the chromospheric layer up to temperatures $T \approx 10^6$–10^8 K and generating enhanced sub-THz flare emission. However, one would expect coincident temporal profiles of sub-THz, microwave, and X-ray emission in the impulsive phase of the flare, which is not always observed (Smirnova et al., 2021).

The mechanism of STF emission may be of a composite nature, which includes both magnetobremsstrahlung emission from optically thick extended flare ribbons and nonthermal emission from compact regions that are under conditions anomalous for the chromosphere. The available observational data are insufficient to elucidate the nature of STFs; therefore, new multiwavelength flare observations are required to fill in the W-shaped spectrum of STFs as completely as possible.

The aim of the present work is to examine the feasibility of sub-THz observations with the RATAN-600 radio telescope.

2 On the feasibility of sub-THz observations with RATAN-600

A method for solar tracking with RATAN-600 using a reduced aperture of 100–120 m was proposed and first tested by Khaikin et al. (2000). In its present-day multi-azimuth modification, the method enables solar tracking with a feed and scanning with a carriage over 8–12 minutes at each of 16–20 azimuths of the South+Flat antenna system (AS), with an azimuth interval of 4° and a maximum daily solar observation duration of 4–5 hours (Khaikin et al., 2018). A sufficiently high tracking accuracy for the type-3 feed and its carriage has been achieved through the modernization of the antenna control system (ACS; Storozhenko et al., 2021). It is planned to further equip the ACS with a high-precision inertial navigation system incorporating two spatially separated global navigation satellite system (GNSS) antennas developed by the Laboratory of Microdevices (Zelenograd), which will provide autonomous angular rate and position feedback from the feed ACS (Khaikin et al., 2023).

The instrumental feasibility of STF observations with RATAN-600 is examined in Khaikin et al. (2023). For STF observations in the millimeter (mm) wavelength range, it is proposed to use a substantially reduced telescope aperture, illuminating a single group of elements (25 shields) within a sector consisting of 7 shield groups. The optimal wavelengths for STF observations in the mm wavelength range with RATAN-600 are 10 and 3 mm, given the fact that the telescope operates in standard mode with satisfactory antenna efficiency up to a wavelength of 10 mm.

An important factor in STF observations is the accounting for mm signal absorption in the Earth's atmosphere.

The radio transparency of the atmosphere in the mm wavelength range is determined by water vapor content, liquid water in clouds, and oxygen. The contribution of oxygen away from its absorption lines is less significant and can be calculated accounting for the altitude of the site and the surface pressure. Efficient observations in the short mm wavelength range require the monitoring of radio transparency or optical depth of the atmosphere. In Khaikin (2023), a radiometric method was proposed for measuring the atmospheric optical depth during solar tracking with RATAN-600 at wavelengths of 3 and 2 mm. The optical depth of a clear atmosphere is directly proportional to the atmospheric water vapor content, while that of a cloudy atmosphere is directly proportional to the cloud liquid water content. The proportionality coefficients for these contributions are the specific absorption coefficients in water vapor and liquid water that depend on wavelength, season, and altitude of the site (Bubnov et al., 2020).

It should be noted that the daily mean atmospheric absorption in the 2–3 mm range under favorable meteorological conditions (absence of rain, fog, snow, and thunderstorm clouds) is typically no more than 0.1/0.2 neper (Np) even at low-altitude sites, reducing the solar flux by no more than 10–25%. Of greater importance are short-term variations in atmospheric absorption, which can attenuate the solar flux by 40–50% in particular due to clouds or changes in atmospheric water vapor content. Monitoring of atmospheric water vapor and cloud cover is therefore essential for STF observations since slow and rapid atmospheric absorption variations ranging from seconds to minutes can in some cases be difficult to distinguish from variations in the solar flux.

For atmospheric water vapor monitoring, the GNSS method described in Shihovtsev et al. (2022) was proposed. In this method, the water vapor content is estimated from the computation of a delay of signals propagating from the satellite to the receiver, caused by tropospheric refraction. A GNSS receiving station and a meteorological station equipped with a solar photometer (pyranometer) have been installed at

RATAN-600 for atmospheric water vapor and cloud monitoring.

Previously, in the 1990s, sporadic solar observations at a wavelength of 3.2 mm were acquired with RATAN-600, conducted primarily for methodological purposes to assess the quality of mutual alignment of antenna elements via solar wavefronts and the quality of the reflecting surface via the scattered sky background (Gosachinskii et al., 1989). Examination of historical records of solar transit curves, performed with a recorder with minute time stamps using individual RATAN-600 shields in 1987 for the assessment of their reflecting surface quality, demonstrates that active regions (ARs) on the Sun at a wavelength of 3.2 mm can be prominent by these shields and monitored over several days (Fig. 1).

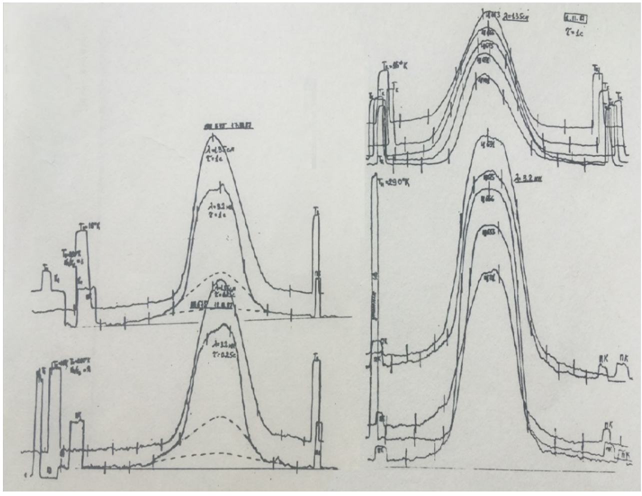

Fig. 1. Records of solar transit curves derived with individual RATAN-600 shields for assessing their reflecting surface quality at wavelengths of 1.35 cm and 3.2 mm in 1987.

The principal feasibility of observations with RATAN-600 at a wavelength of 2 mm, from the standpoint of systematic and random error contributions, is demonstrated in Majorova (1987) with the recommendation to illuminate only central parts of the shields in this range. However, this will require new efforts to improve the reflecting surface quality of the shields, analogous to those undertaken previously in the 1990s.

STF observations are proposed to be carried out in the course of routine multi-azimuth solar observations in the cm wavelength range with the RATAN-600 South+Flat AS in transit mode with a full aperture at a wavelength of 10 mm and with a reduced aperture (50 m) at a wavelength of 3 mm. Periodic observations are also implied in solar tracking mode with a reduced aperture of 100×5 m at a wavelength of 10 mm and 50×2 m at a wavelength of 3 mm. For this purpose, it is proposed to employ conical horns with a half-width of the beam patterns of 7° at a wavelength of 3 mm, developed by MWAVE LLC (Khaikin et al., 2023). The effective horizontal aperture size will thereby be ~50 m, providing sufficiently high spatial resolution of solar ARs and substantially simplifying instrument operation at such a short wavelength.

The root-mean-square (RMS) surface deviation of the central 2×2 m part of the RATAN-600 shields, 25 years after their last recoating, does not exceed 0.35 mm, allowing for observation of discrete solar sources with a mean antenna RMS of 0.5–0.6 mm at a reduced aperture of 50 m. The antenna efficiency of the reduced aperture in the 3–10 mm range is ~2–15%. Within 10 years after the new surface recoating, the RMS of the central part of the shields of the circular and flat reflectors does not exceed 0.1 mm, while the RMS of the central part of the secondary mirror can be achieved at no worse than 0.1 mm using laser geodetic methods. As a result of special antenna preparation, the integral surface RMS at the South+Flat AS can be reduced to 0.3 mm, enabling STF observations at wavelengths of 3 and 2 mm with a reduced aperture antenna efficiency of ~20.4% and a full aperture efficiency of ~30% at 10 mm. The antenna efficiency of the reduced aperture (100–120 m) at a wavelength of 10 mm is reduced by a factor of 1.5–2 due to full horizontal and vertical illumination of the antenna sector.

To achieve a RMS value of the mutual alignment of antenna elements of 0.15 mm, it is proposed to use a fast radio holographic method with radial motion of the reference element. This can be performed at a wavelength of 10 mm in autocollimation (AC) mode or using the geostationary satellite (GS) Express AMU1 at a wavelength of 1.5 cm in the operational antenna position. Control of AC focal spots can be performed at wavelengths of 3–4 mm (Khaikin et al., 2018). For this purpose, highly stable signal sources based on frequency synthesizers at wavelengths of 4 and 3 mm have been developed by MWAVE LLC (Khaikin et al., 2023). A scalar horn antenna operating at 75–110 GHz developed by Skard Electronics JSC (Kursk) may be used to illuminate a large part of the South+Flat AS sector. The antenna beam pattern width is 45° at the −10 dB level. In this context, we aim to explore the feasibility of STF observations at wavelengths of 10 mm and 3 mm without special antenna preparation and with the primary feeds placed off-focus during routine observations. This will inevitably reduce the beam pattern quality, antenna efficiency in the mm wavelength range, and flux sensitivity of the instrument, but will enable daily solar flare monitoring. As a consequence, this will allow more frequent detection of STFs with flux densities exceeding 100 sfu at a wavelength of 3 mm. Nevertheless, a number of preparatory antenna procedures are absolutely essential for STF observations in addition to routine autocollimation alignments of the primary mirror at a wavelength of 1.8 cm, focal spot measurements at 8 mm, and kinematic corrections of individual shields using laser geodetic methods. The "calibration" (refinement) of the longitudinal focus of the AS for the type-3 feed at different azimuths is principally required, which can be performed using the GS Turksat 3A (42° East) in the Ku-band, the GS Express AMU1 (36° E) in the Ka-band, etc.

Figure 2 presents an example of this procedure carried out at 11.9 GHz in 2014, where the focus offset amounted to 6 mm. The curves shown appear to decline slowly with offsetting longitudinal focus; however, at a wavelength of 3 mm they will decline nearly an order of magnitude more rapidly. It is also necessary to correct for the systematic rotation of the secondary mirror of the type-3 feed relative to the normal to the longitudinal axis, which gives rise to

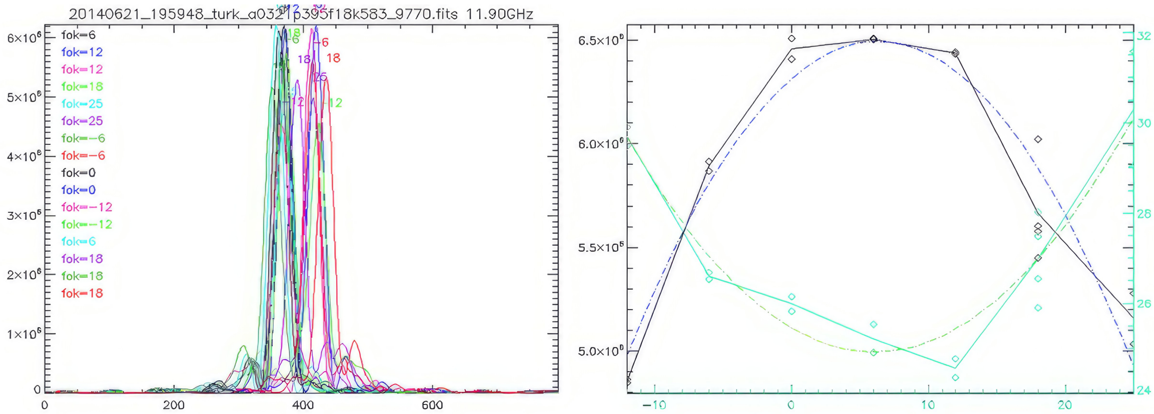

Fig. 2. Example of longitudinal focus "calibration" (refinement) of the AS using the GS Turksat 3A: a beam pattern with longitudinal focus offset (left), amplitude and half-width of the beam pattern (right).

substantial cubic coma aberration, requiring effort from the radio telescope operation staff.

For solar flux calibration at a wavelength of 10 mm and longer, the radio galaxy 3C274 with its compact Virgo A source and well-established flux density of 21.6/16.8/7.8 Jy at 22.68/32.94/92.89 GHz can be used. Brightness temperature calibration of solar observations in the cm and mm wavelength ranges is conveniently performed using the Moon. Beam pattern measurements of the AS in the 3–4 mm range can be carried out using the operational low-Earth orbit (flyby) experimental W-band satellite W-Cube.

For STF observations, it is proposed to use commercially available compact direct-amplification radiometric modules in the W-band and, prospectively, the D-band, developed for radio imaging with a fluctuation sensitivity in total-power mode of no worse than 0.1–0.2 K/Hz^2 (Khaikin et al., 2023). Based on the expected bands of receivers, their centers correspond to wavelengths of 3.3 and 2.14 mm.

3 Results of modeling the RATAN-600 characteristics and expected images of STFs on the Sun

To assess the feasibility of such short-wavelength observations, the expected beam patterns of the South+Flat AS have been computed at wavelengths of 10, 3, and 2 mm, accounting for possible surface errors of the elements, errors in their mutual alignment, and the primary feed placed off-focus, as well as the two-dimensional convolutions with the solar model with a source; the one-dimensional scans of these convolutions correspond to the expected solar radio images acquired with RATAN-600. In Khaikin et al. (2023), a method was proposed for computing the beam pattern of the RATAN-600 South+Flat AS in the mm wavelength range, accounting for possible errors of the antenna surface and the primary feed off-focus. According to the Rayleigh–Jeans law, the integrated thermal STF flux can be expressed as (Kontar et al., 2018)

$$F = \frac{2\nu^2 k_B T}{c^2}\frac{A}{R^2} \simeq 772\left(\frac{\nu}{100\ \mathrm{GHz}}\right)^2\left(\frac{T}{10^6\ \mathrm{K}}\right)\left(\frac{A}{10^3\ \mathrm{arcsec}^2}\right)[\mathrm{sfu}], \quad (1)$$

where k_B is the Boltzmann constant, ν is the frequency, c is the speed of light, T is the effective temperature, A is the projected area of the radio source on the solar disk, R is the Sun–Earth distance, and [sfu] denotes solar flux units. For temperatures $T = 10^4, 10^5, 10^6$ K and $A \approx 1000$ arcsec^2, the flux densities are $F(30\,\mathrm{GHz}) = 649.80, 6498, 64980$ sfu, $F(93\,\mathrm{GHz}) = 662.445, 6624.45, 62445$ sfu, $F(140\,\mathrm{GHz}) = 1415.12, 14151.2, 141512$ sfu under the assumption of an optically thick source for which the brightness temperature $T_b = T$. The expected instrument sensitivity is given by

$$\Delta F = \frac{2k_B \Delta T_a}{S_{\mathrm{eff}}}, \quad (2)$$

where ΔT_a is the telescope antenna temperature sensitivity (2 K), and S_{eff} is the expected effective antenna area (taking achievable values: for a wavelength of 10 mm and aperture of 100 m, $S_{\mathrm{eff}} = 85$ m^2; for a wavelength of 3.3 mm and aperture of 50 m, $S_{\mathrm{eff}} = 20$ m^2; for a wavelength of 2.15 mm and aperture of 50 m, $S_{\mathrm{eff}} = 4$ m^2). The achievable sensitivity after antenna alignment and focus calibration is $\Delta F(10\ \mathrm{mm}) \sim 0.025$ sfu, $\Delta F(3.3\ \mathrm{mm}) \sim 1$ sfu, $\Delta F(2.15\ \mathrm{mm}) \sim 30$ sfu, and with a minimum possible off-focus of 7–12 cm: $\Delta F(10\ \mathrm{mm}/13\ \mathrm{cm}) \sim 0.05$ sfu, $\Delta F(3.3\ \mathrm{mm}/10\ \mathrm{cm}) \sim 2$ sfu, $\Delta F(2.14\ \mathrm{mm}/7\ \mathrm{cm}) \sim 60$ sfu. However, according to our estimates, without the aforementioned preparatory antenna procedures, the actual flux sensitivity at a wavelength of 10 mm is several times worse, while at 3.3 mm it is an order of magnitude worse.

Figure 3 presents the computed one-dimensional and two-dimensional beam patterns. However, the practical implementation of regular STF observations at focus, where the standard solar complex feed is normally located, is not feasi-

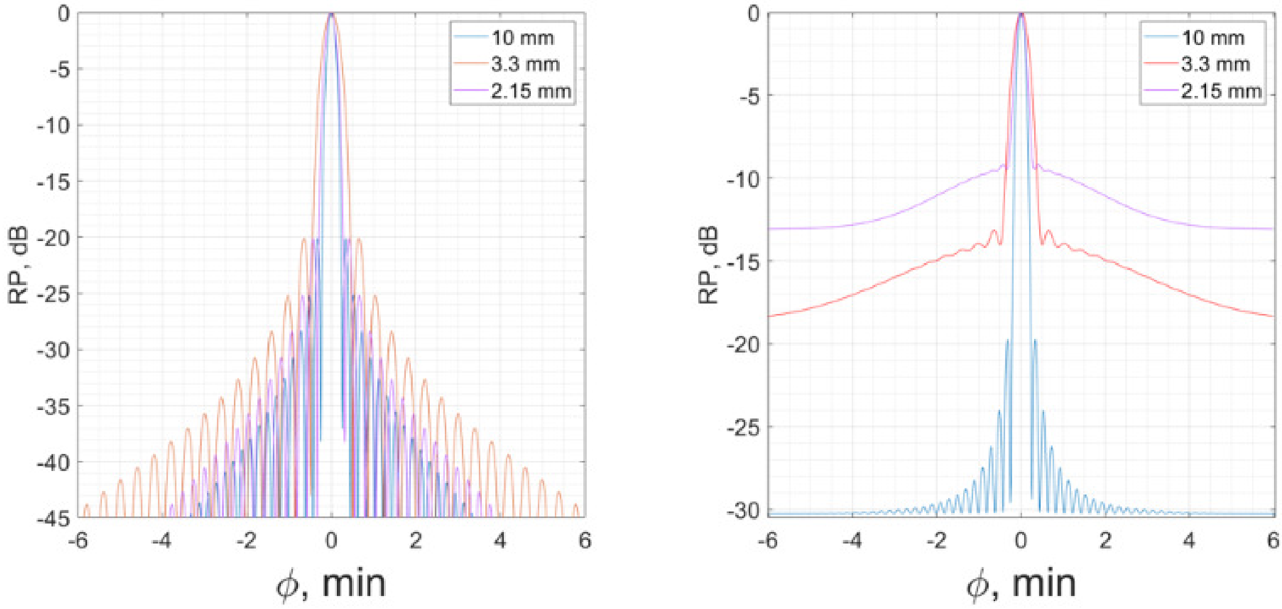

Fig. 3. Beam pattern cross-sections in the spherical coordinate ϕ at wavelengths of 10, 3.3, and 2.14 mm with errors (right) and without errors (left).

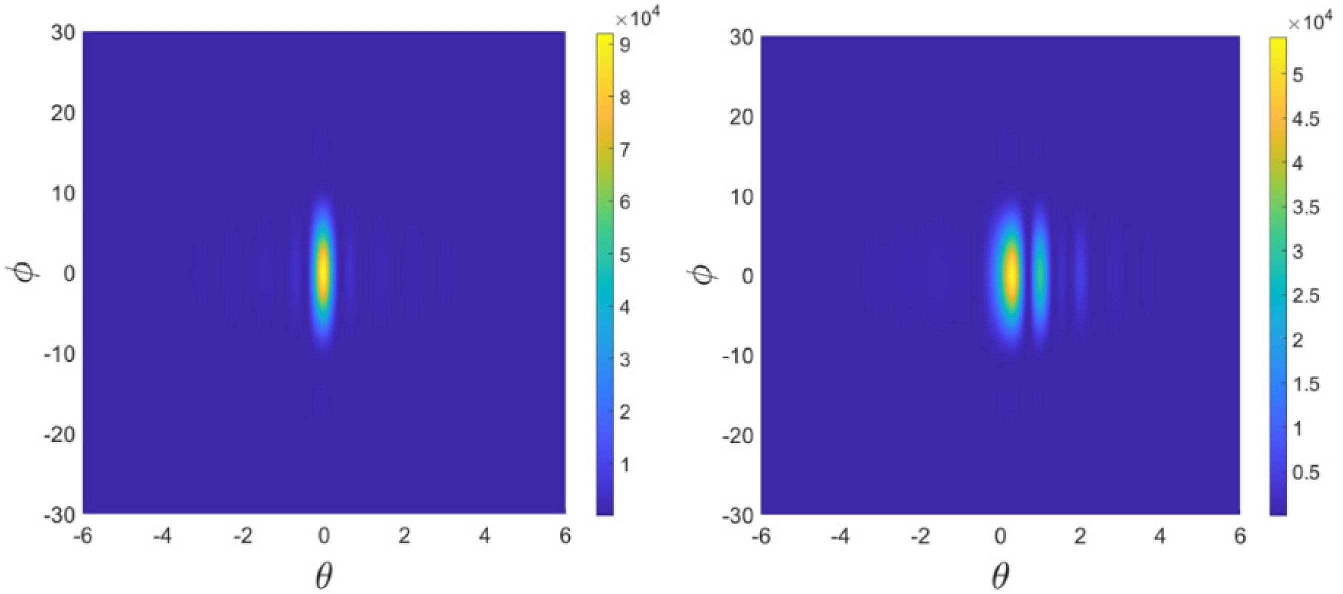

Fig. 4. Two-dimensional beam patterns with the receiver placed off-focus at a distance of 12 cm (right) and without off-focus (left).

ble. STF observations off focus lead to distortion of the beam pattern shape and attenuation of the source signal. Figures 4–7 present the beam patterns off focus. Distortions of the beam pattern shape are not critical since they can be modeled; however, signal power losses along the propagation path will result in a flux sensitivity degradation of ~2 times at a wavelength of 10 mm with an aperture of 100 m, and ~2 times at a wavelength of 3.3 mm with an aperture of 50 m. Figures 8–9 present convolutions between the solar model for a sufficiently compact disk-shaped source with $T_b = 10^5$ K and the computed beam patterns. Two-dimensional convolutions are not entirely abstraction for the RATAN-600 South+Flat AS. They can be obtained in practice during solar tracking with the feed by scanning the Sun with a carriage carrying the receivers and varying the height of the flat reflector after each scan. The result is a two-dimensional solar map analogous to those shown in Figs. 8–9. The time required to produce such a map with ten solar scans made by the carriage is ~10 minutes. Analysis of such a map at the beginning of daily solar observations can be useful for identifying the AR exhibiting

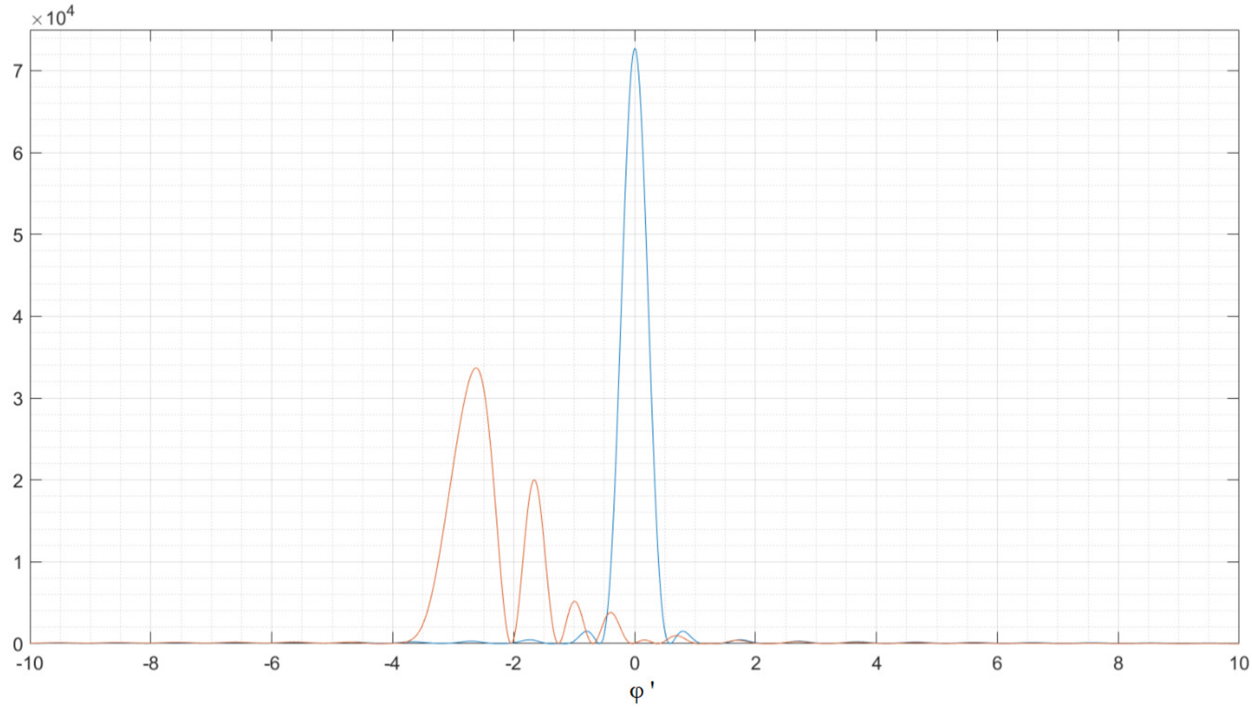

Fig. 5. Beam pattern for the 100-m aperture at a wavelength of 10 mm with the receiver placed off-focus at a distance of 12 cm (red curve) and without off-focus (blue curve).

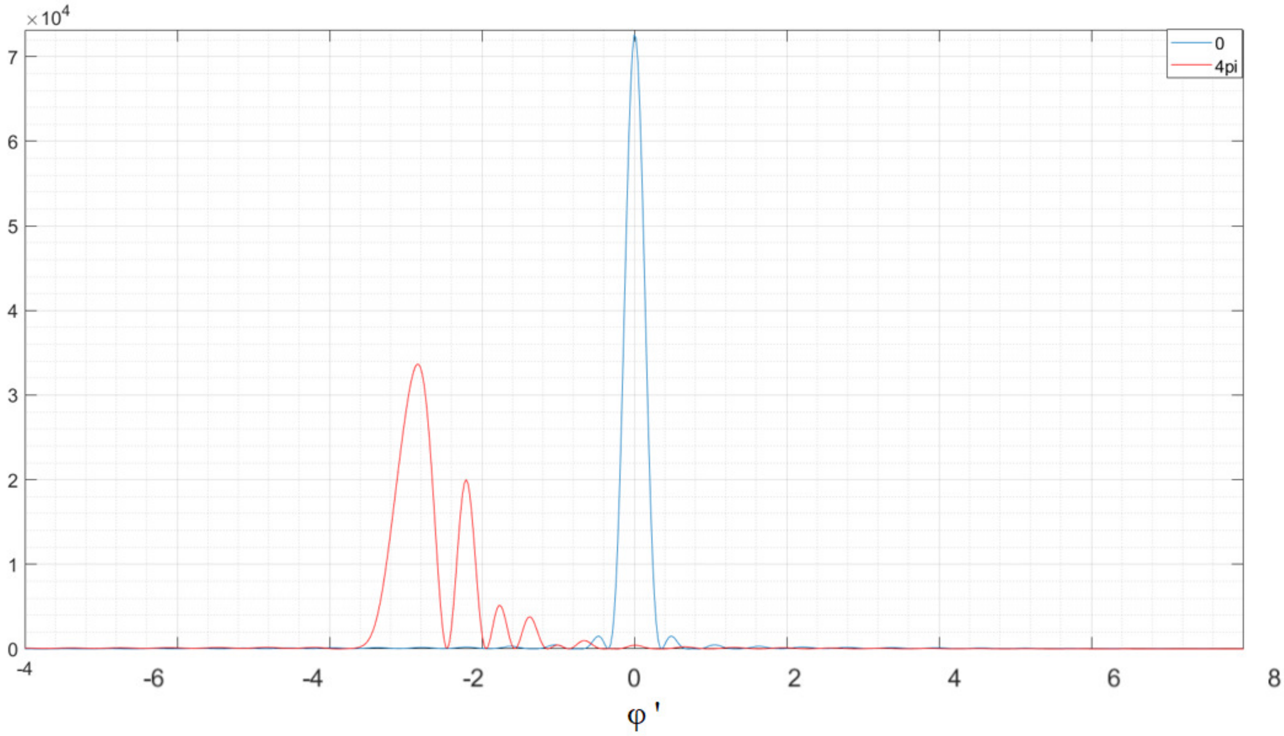

Fig. 6. Beam pattern for the 50-m aperture at a wavelength of 3.3 mm with the receiver placed off-focus at a distance of 10 cm (red curve) and without off-focus (blue curve).

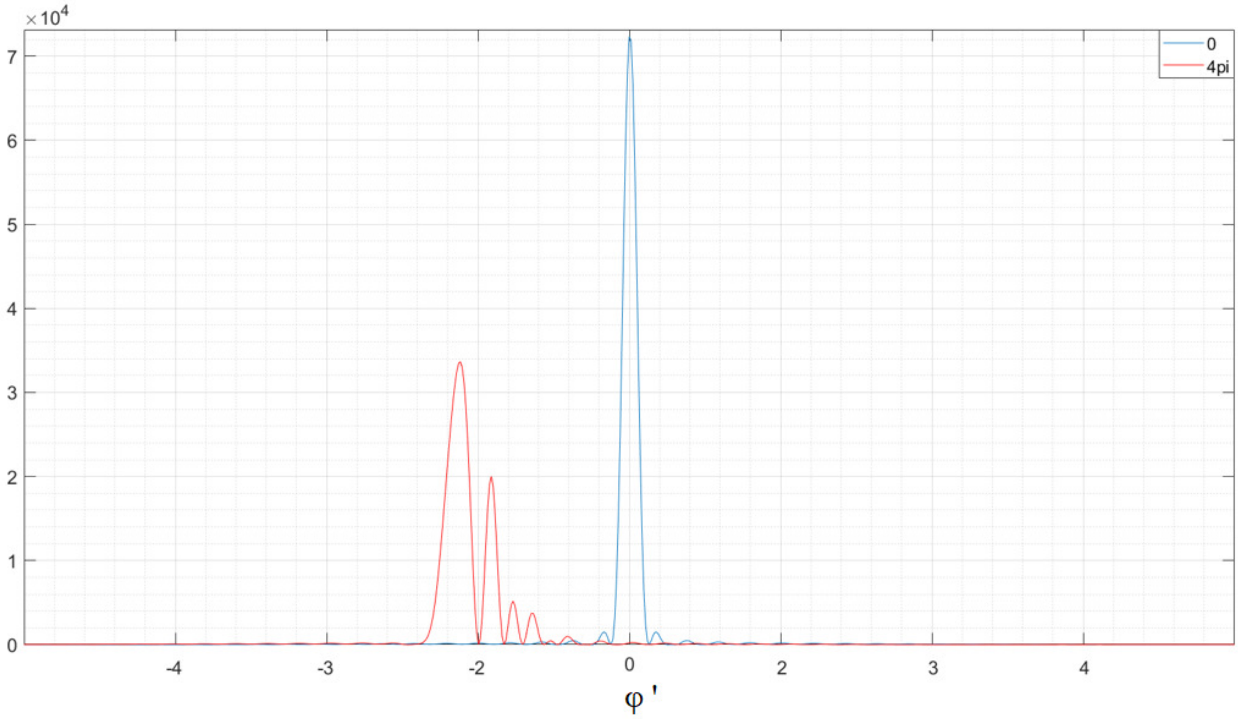

Fig. 7. Beam pattern for the 50-m aperture at a wavelength of 2.14 mm with the receiver placed off-focus at a distance of 7 cm (red curve) and without off-focus (blue curve).

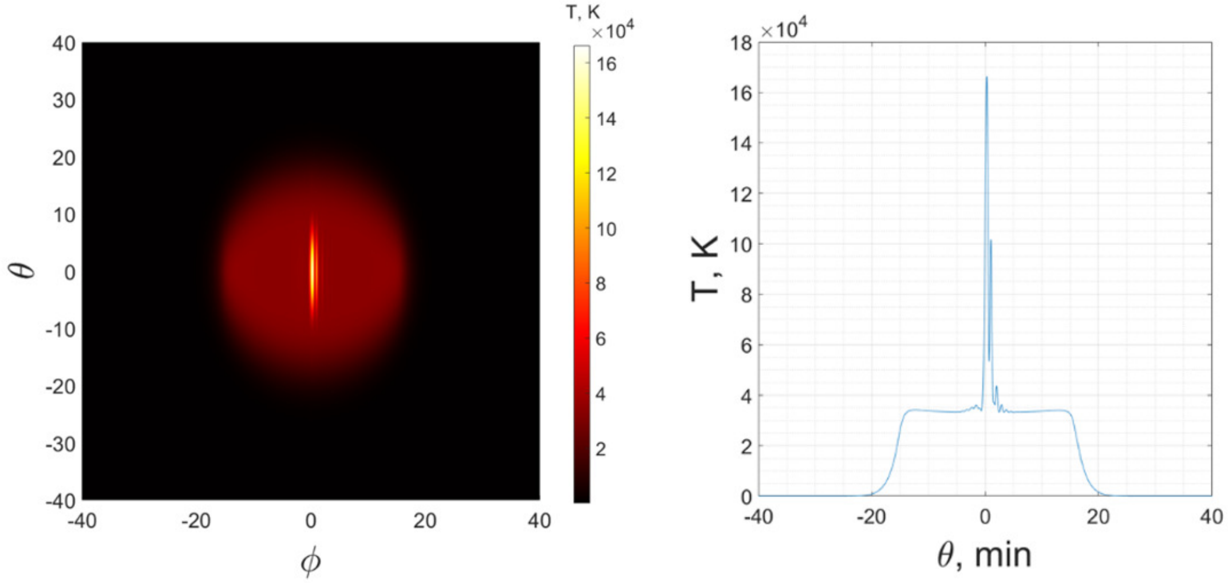

Fig. 8. Convolution between the solar model with a compact disk-shaped source and the coma beam pattern (10λ off-focus) at a wavelength of 10 mm (120-m aperture).

the highest contrast at a wavelength of 10 mm, enabling its subsequent monitoring in multi-azimuth transit or tracking mode.

Figure 9 demonstrates that the 2 mm wavelength is ineffective for STF observations in the current state of the radio telescope and requires substantial improvement of the reflecting surface quality.

3.1 Expected rate and observational plans for STFs

An important issue for us concerns the occurrence rate of STFs. In Kontar et al. (2018), only 16 STFs with a positive spectral slope are described for the period between 2000 and 2014; however, these are only the events that were successfully observed and published. In March 2022, 146 solar flares

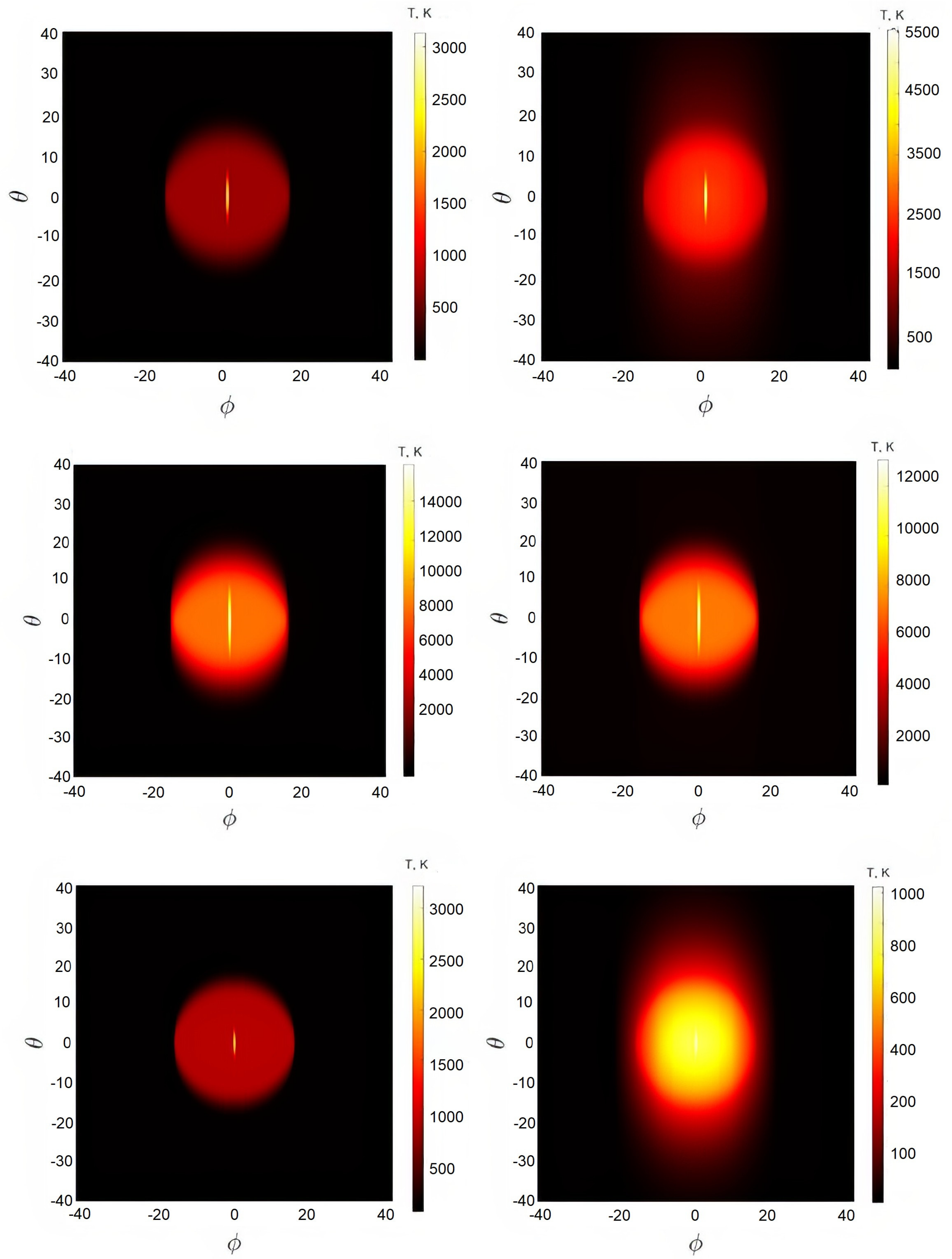

Fig. 9. Convolutions between the solar model with limb brightening and a compact disk-shaped source and the beam patterns derived at a wavelength of 10 mm (top), 3.3 mm (middle), and 2.15 mm (bottom) with errors (right) and without errors (left).

occurred, including 14 flares of X-ray class M. On average, more than 100 M-class and 10 X-class flares occur per year during solar activity maximum.

The main reasons for the insufficient amount of sub-THz observational data for reliable interpretation are the high requirements to the parameters of receiving instrumentation and the antenna system of radio telescopes, in particular the antenna surface accuracy, receiver sensitivity, methods for determining signal absorption in the Earth's atmosphere, as well as the challenges of primary calibration and data reduction. The complexity of technical solutions and difficulties in selecting optimal sites for short-wavelength radio telescopes limit the number of high-quality sub-THz observations. Therefore, in view of ongoing developments in new models of the flare process and the nature of solar activity, regular sub-THz observations combined with multiwavelength data in other ranges are still relevant.

In 2022, more than 60 STFs of X-ray classes C and M were recorded at 93 GHz with the Bauman Moscow State Technical University RT-7.5 radio telescope, indicating a sufficiently high probability of such events (Ryzhov et al., 2023). All M-class flares observed with RT-7.5 at two frequencies (93 and 140 GHz) were found to be sub-THz events (a positive spectral slope was observed between 93 and 140 GHz). According to SST observations (212 and 405 GHz), approximately 25% of all observed flares are sub-THz events with a positive spectral slope (Fernandes et al., 2017).

In recent years, the first STFs with a positive spectral slope have been detected for various stars, including Proxima Centauri. This has been made possible through the use of optical and radio telescopes, including the Atacama Large Millimeter/submillimeter Array (ALMA) radio interferometer operating at a wavelength of 1.3 mm with both linear and circular polarization (MacGregor et al., 2021). This approach motivates high-spatial-resolution polarimetric STF observations on the Sun. A solar receiver for measuring circular polarization at 30–40 GHz is currently under development for RATAN-600. In view of the capability for regular STF observations with RT-7.5 at a flux sensitivity of no worse than 0.01 sfu, it has been proposed to conduct cooperative synchronous STF observations with the Bauman Moscow State Technical University RT-7.5 mm-wavelength radio telescope and RATAN-600 at 1–100 GHz, enabling refinement of the W-shaped spectrum of STFs in the decimeter (dm), cm, and mm wavelength ranges. In particular, simultaneous polarimetric observations are planned to be carried out with both RATAN-600 at 1–3 GHz with circular polarization and high frequency and temporal resolution at frequencies of 4.7, 8.3, 30, and 93 GHz and RT-7.5 at frequencies of 93 and 140 GHz.

4 Conclusions

The RATAN-600 South+Flat AS with a reduced (50–100 m) aperture can be used for STF observations with a positive spectral slope at wavelengths of 10 and 3 mm. STF observations at 2 mm require new efforts to improve the reflecting surface quality of the shields, analogous to those undertaken in the 1990s.

As demonstrated by modeling of the antenna characteristics accounting for surface errors and the feed off-focus, the actual solar flux sensitivity today may reach 1–2 sfu at a wavelength of 3.3 mm in the course of a number of preparatory antenna procedures. The primary preparatory procedure is the "alignment" (refinement) of the longitudinal focus of the AS for the type-3 feed at different azimuths using the GS Turksat 3A/4A (42° E) in the Ku-band, the GS Express AMU1 (36° E) in the Ka-band, and other GSs, as well as a precise alignment of the secondary mirror normal to the longitudinal axis of the AS, which will fundamentally improve the antenna characteristics of the instrument at a wavelength of 3 mm. The next critical observational technique is fast radio holographic antenna adjustment using the GS Express AMU1 at a wavelength of 1.5 cm, followed by controlling the antenna characteristics at 3–4 mm in AC mode and using the flyby satellite W-Cube. The brightness temperature calibration of RATAN-600 solar observations in the cm- and mm wavelength ranges can be conveniently performed using the Moon.

Given the capability for regular solar observations with RT-7.5 at 93 and 140 GHz, it is highly advisable to conduct STF observations in cooperation with RATAN-600 at 1–100 GHz, which will enable refinement of the W-shaped spectrum of STFs in the dm-, cm-, and mm wavelength ranges.

This work was carried out within the framework of the state assignment of SAO RAS approved by the Ministry of Science and Higher Education of the Russian Federation and supported by the RFBR grant 20-52-26006 Czech_a (V.V. Smirnova).

References

Bubnov G., Vdovin V., Khaikin V., Tremblin P., Baron P., 2020. Proceedings of 7th Russian Microwave Conference, pp. 229–232.
Clark C.D., Park W.M., 1968. Nature, vol. 219, p. 922.
Gosachinskii I.V., Majorova E.K., Pariiskii Yu.N., 1989. SAO reports, no. 63, pp. 38–49. (In Russ.)
Fernandes L.O.T., Kaufmann P., Correia E., et al., 2017. Solar Phys., vol. 292, iss. 1, id. 21.
Fleishman G.D., Kontar E.P. 2010. Astrophys. J. Lett., vol. 709, L127.
Kaufmann P., Trottet G., Giménez de Castro C.G., et al., 2000. Solar Phys., vol. 197, iss. 2, pp. 361–374.
Kaufmann P., Trottet G., Giménez de Castro C.G., et al., 2009. Solar Phys., vol. 255, iss. 1, pp. 131–142.
Khaikin V.B., 2023. Proceedings of XXIX International conference "Atmospheric and ocean optics", p. A-361. (In Russ.)
Khaikin V.B., Majorova E.K., Efimov I.G., Victorov O.A., 2000. Astron. Astrophys. Trans., iss. 3–4, pp. 596–611.
Khaikin V.B., Lebedev M.K., Ripak A.M., 2018. Trans. Inst. Appl. Astron. RAS, no. 47, pp. 48–63. (In Russ.)
Khaikin V.B., Makoev G.A., Storozhenko A.A., Murav'ev V.M., 2023. Proceedings of the All-Russian conference "REDS-2023", p. 57. (In Russ.)
Kontar E.P., Motorina G.G., Jeffrey N.L.S., et al., 2018. Astron. Astrophys., vol. 620, id. A95.
Krucker S., Giménez de Castro C.G., Hudson H.S., et al., 2013. Astron. Astrophys. Rev., vol. 21, id. 58.
Kundu M.R., Vlahos L. 1982. Space Sci. Rev., vol. 32, iss. 4, p. 405.

Kupriyanova E.G., Kolotkov D.Yu., Nakariakov V.M., Kaufman A.S., 2020. Solar-terrestrial physics, vol. 6, no. 1, pp. 3–29. (In Russ.)

Lüthi T., Magun A., Miller M., 2004. Astron. Astrophys., vol. 415, pp. 1123–1132.

MacGregor M.A., Weinberger A.J., Loyd R.O.P., et al., 2021. Astrophys. J. Lett., vol. 911, p. L25.

Majorova E.K., 1987. SAO reports, no. 25, pp. 135–142. (In Russ.)

Ryzhov V.S., Shivrina P.V., Smirnova V.V., 2023. Izv. Krimsk. Astrofiz. Observ., vol. 119, no. 1, pp. 11–18. (In Russ.)

Shihovtsev A.Yu., Khaikin V.B., Mironov A.P., Kovadlo P.G., 2022. Optika atmosfery i okeana, vol. 35, no. 1, pp. 67–73. (In Russ.)

Skokić I., Benz A.O., Brajša R., et al., 2023. Astron. Astrophys., vol. 669, p. A156.

Smirnova V.V., Tsap Yu.T., Morgachev A.S., Motorina G.G., Bárta M., 2021. Geomagnetism and Aeronomy, vol. 61, iss. 7, pp. 993–1000.

Stepanov A.V., 2019. Proceedings of the Baikal young scientists' international school on fundamental physics, pp. 30–34. (In Russ.)

Storozhenko A.A., Bogod V.M., Lebedev M.K., et al., 2021. Proceedings of XXV All-Russian conference "Solar and solar-terrestrial physics – 2021", p. 253. (In Russ.)

Tsap Yu.T., Smirnova V.V., Morgachev A.S., et al., 2016. Adv. Space Res., vol. 57, iss. 7, pp. 1449–1455.

Tsap Yu.T., Smirnova V.V., Motorina G.G., Morgachev A.S., Kuznetsov S.A., Nagnibeda V.G., Ryzhov V.S., 2018. Solar Phys., vol. 293, iss. 3, id. 50.

Zaitsev V.V., Stepanov A.V., 2015. Solar Phys., vol. 290, iss. 12, pp. 3559–3572.